Biosensors and Bioelectronics 178 (2021) 113027

Contents lists available at ScienceDirect

Biosensors and Bioelectronics

journal homepage: http://www.elsevier.com/locate/bios

A CRISPR/Cas13a-powered catalytic electrochemical biosensor for successive and highly sensitive RNA diagnostics

Yan Sheng [a,b,1], Tenghua Zhang [a,b,1], Shihong Zhang [c,1], Midori Johnston [d,e], Xiaohe Zheng [c], Yuanyue Shan [a,b], Tong Liu [f], Zena Huang [g], Feiyang Qian [a,b], Zihui Xie [a,b], Yiru Ai [a,b], Hankang Zhong [a,b], Tairong Kuang [f,*], Can Dincer [d,e,**], Gerald Anton Urban [e], Jiaming Hu [a,b,***]

[a] MOE Key Laboratory of Laser Life Science & Institute of Laser Life Science, Guangdong Provincial Key Laboratory of Laser Life Science, South China Normal University, Guangzhou, 510631, China
[b] College of Biophotonics, South China Normal University, Guangzhou, 510631, China
[c] Department of Clinical Laboratory, The First Affiliated Hospital, Sun Yat-sen University, Guangzhou, 510080, China
[d] Freiburg Center for Interactive Materials and Bioinspired Technologies – FIT, University of Freiburg, Georges-Koehler Allee 105, 79110, Freiburg, Germany
[e] Department of Microsystems Engineering – IMTEK, Laboratory for Sensors, University of Freiburg, Georges-Koehler Allee 103, 79110, Freiburg, Germany
[f] College of Materials Science and Engineering, Zhejiang University of Technology, Hangzhou, 310014, China
[g] Department of General Medicine, Guangdong Provincial People's Hospital, Guangdong Academy of Medical Sciences, Guangzhou, 510080, China

ARTICLE INFO

Keywords:
CRISPR/Cas technology
On-site testing
Nucleic acid diagnostics
Catalytic hairpin
DNA circuit
Electrochemical analysis

ABSTRACT

Rapid and specific quantitation of a variety of RNAs with low expression levels in early-stage cancer is highly desirable but remains a challenge. Here, we present a dual signal amplification strategy consisting of the CRISPR/Cas13a system and a catalytic hairpin DNA circuit (CHDC), integrated on a reusable electrochemical biosensor for rapid and accurate detection of RNAs. Signal amplification is accomplished through the unique combination of the CRISPR/Cas13a system with CHDC, achieving a limit of detection of 50 aM within a readout time of 6 min and an overall process time of 36 min, using a measuring volume of 10 μL. Enzymatic regeneration of the sensor surface and ratiometric correction of background signal allow up to 37 sequential RNA quantifications by square-wave voltammetry on a single biosensor chip without loss of sensitivity. The reusable biosensor platform could selectively (specificity = 0.952) and sensitively (sensitivity = 0.900) identify low expression RNA targets in human serum, distinguishing early-stage patients (n = 20) suffering from non-small-cell lung carcinoma (NSCLC) from healthy subjects (n = 30) and patients with benign lung disease (n = 12). Measurement of six NSCLC-related RNAs (miR-17, miR-155, TTF-1 mRNA, miR-19b, miR-210 and EGFR mRNA) shows the ability of the electrochemical CRISPR/CHDC system to be a fast, low-cost and highly accurate tool for early cancer diagnostics.

1. Introduction

Rapid detection of minute amounts of nucleic acids, especially microRNAs (miRNAs) and messenger RNAs (mRNAs) on miniaturized devices could drastically improve the patient's disease outcome by enabling timely diagnostics and treatment monitoring. miRNAs regulate gene expression by binding to their target mRNAs and promoting their degradation or translational inhibition (Guo et al., 2010; Hausser and Zavolan 2014). mRNAs, being located at the key position between genome and proteome, encode the genetic information necessary for protein synthesis (Muers 2011; Proudfoot et al., 2002; Wickramasinghe and Laskey 2015). In the past years, miRNAs and mRNAs have gained considerable attention as biomarkers, since their aberrant expression is closely associated with the occurrence and development of multiple

* Corresponding author. College of Materials Science and Engineering, Zhejiang University of Technology, Hangzhou, 310014, China.
** Corresponding author. Freiburg Center for Interactive Materials and Bioinspired Technologies – FIT, University of Freiburg, Georges-Koehler Allee 105, 79110, Freiburg, Germany.
*** Corresponding author. MOE Key Laboratory of Laser Life Science & Institute of Laser Life Science, Guangdong Provincial Key Laboratory of Laser Life Science, South China Normal University, Guangzhou, 510631, China.
E-mail addresses: kuangtr@zjut.edu.cn (T. Kuang), dincer@imtek.de (C. Dincer), jmhu@m.scnu.edu.cn (J. Hu).
[1] These authors contributed equally.

https://doi.org/10.1016/j.bios.2021.113027
Received 17 September 2020; Received in revised form 8 January 2021; Accepted 20 January 2021
Available online 23 January 2021

diseases, such as cancer or cardiovascular disorders (Hu and Kuang 2018; Hu et al., 2017; Jeffrey 2008; Santarius et al., 2010; Vanlandewijck et al., 2018; Yanaihara et al., 2006). The abundance of particular miRNA or mRNA sequences can vary from a single copy to more than 50, 000 copies in a sample of interest (Bartel 2004), thus requiring exceptional sensitivity, especially for early-stage diagnosis. The traditional methods for measuring RNAs, such as quantitative reverse transcription polymerase chain reaction (qRT-PCR), next-generation sequencing and microarrays, generally rely on bulky and expensive equipment, complex sample preparation and long sample-to-result times, which restrict them to well-equipped laboratories and limit their broad application. Therefore, it is vital to develop rapid, portable, highly specific and sensitive strategies for RNA detection at the point of care (POC).

Biosensing devices offer rapid, highly specific and sensitive quantification of miRNAs/mRNAs in an inexpensive and simple manner. Herein, one attractive approach is the application of lab-on-a-chip (LOC) devices, commonly paired with either an optical or electrochemical signal readout. LOC biosensing platforms based on optical detection are low-cost, easy-to-handle and fast (Gao et al., 2020; Lee et al., 2020; Treerattrakoon et al., 2019), however, they either lack sensitivity, or require a non-disposable and comparably bulky reader for the signal amplification and/or readout. On the other hand, electrochemical readout techniques are employed in a wide range of biosensors because of their high sensitivity and potential for high-level miniaturization for POC testing (Bruch et al., 2019a; Dincer et al., 2017; Dittrich and Manz 2006; Heller and Feldman 2008). However, an obstacle in the way of the wider adoption of many electrochemical biosensors as diagnostic devices is their baseline drift problem. This is mostly due to the variability between measurements originating from the alteration of the electrode's surface area by application of functional molecules (e.g., oligonucleotides, proteins, lipids, and etc.) or the unexpected adherence of biomolecules when applied directly in biological matrices (Ferguson et al., 2013). Application of a dual-reporter drift correction, in which one reporter responds to the target, and the other serves as a reference to correct background effects, can improve measurement reproducibility (Li et al., 2016). Furthermore, electrochemical biosensors are limited by their reliance on the single-use surface modifications immobilized on electrodes or fluidic channels (Cai et al., 2010; Hu et al., 2012; Pheeney et al., 2012). Used biosensors have to be disposed of, or their surface modifications must be reconstructed which may require up to a few days, making the use of such biosensors inconvenient and increasing the costs per test. Current washing or magnetic control methods adopted in electrochemical biosensors cannot fully regenerate the sensing interfaces, which leaves the end-users with a risk of crosstalk between samples (Hu et al., 2014; Zhu et al., 2014). Therefore, fast and complete regeneration of the sensing interfaces would facilitate sequential measurements on a single sensor, resulting in minimal interface reconstruction, high-throughput and low-cost, which is critical for the advancement of electrochemical biosensors in clinical applications (Gubala et al., 2012; Hu et al., 2014).

In the recent past, CRISPR/Cas (clustered regularly interspaced short palindromic repeats and CRISPR-associated protein) systems have been exploited as powerful tools for genome editing, transcription regulation and their potential in molecular diagnostics (Bruch et al. 2019b, 2021; Konermann et al., 2015; Tsai et al., 2014). Besides Cas9, which is most commonly used in gene editing (Bruch et al., 2019c; Doudna and Charpentier 2014; Nelles et al., 2016), the cleavage capability of Cas13 for RNAs, Cas12 for single- and double-stranded DNAs and Cas14 for single-stranded DNAs provides great opportunities for CRISPR-based nucleic acid diagnostics (Chen et al., 2018; East-Seletsky et al., 2016; Gootenberg et al. 2017, 2018; Harrington et al., 2018; Li et al., 2018; Shen et al., 2020). These Cas effectors can be easily programmed by a target-specific CRISPR RNA (crRNA) and, thereby, offer an inexpensive, facile and flexible detection of many different targets. An overview of existing CRISPR/Cas-based miRNA detection methods is provided in Supplementary Table 1.

The Winfree group (Seelig et al., 2006; Zhang et al., 2007) first introduced the implementation of functional domains into oligonucleotide sequences, and developed the catalytic hairpin DNA circuit (CHDC). CHDC is an enzyme-free DNA circuit, which facilitates signal amplification by catalyzed hairpin assembly. It consists of two DNA hairpins: hairpin-1, whose allosteric transformations are catalytically triggered by hybridization with a single-stranded nucleic acid, and hairpin-2, which participates in a strand-exchange reaction to displace the single-stranded nucleic acid for the next catalytic cycle. The product of the CHDC is easily detectable by common detection modalities, such as fluorescence, electrochemical or colorimetric detection. In addition, the molecular circuitry of the CHDC provides the opportunity for combination with CRISPR/Cas and an electrochemical sensor to achieve high-level performances. To the best of our knowledge, there has as of yet not been a report on the combination of CRISPR/Cas13a with CHDC to quantify RNAs with high sensitivity.

Herein, we present the Cas-CHDC-powered electrochemical RNA-sensing technology (COMET), which comprises a two-stage signal amplification system integrated on a reusable electrochemical biosensor, for high-sensitivity sequential measurements of various RNAs. Up to now, many miRNAs and mRNAs have been investigated as potential biomarkers for the leading cause of cancer-related death: non-small-cell lung carcinoma (NSCLC) (Lee et al., 2016; Zaporozhchenko et al., 2018). As single biomarker is not sufficient for accurate diagnosis, especially in early-stage cancer (Liu et al., 2019), development of a diagnostic method involving several biomarkers of the same kind (for example: mRNA, miRNA or inflammatory mediators), or even a combination of several different types of biomarkers are needed. Thus, we select a panel of six NSCLC-related RNAs (miR-17, miR-155, TTF-1 mRNA, miR-19b, miR-210 and EGFR mRNA), which are all up-regulated in malignant nodules (Chen et al., 2012; Hu et al., 2018; Lee et al., 2016; Xue et al., 2016; Zaporozhchenko et al., 2018), to validate our assay and compare its performance with qRT-PCR. Our findings demonstrate that the COMET chip is a powerful and easy to use tool for early-stage NSCLC diagnostics.

2. Results

2.1. Overview of the COMET chip

For the electrochemical detection of RNAs, an inexpensive and easy-to-fabricate biosensor chip, as illustrated in Fig. 1A, is manufactured comprising a screen-printed electrode (SPE) setup (a gold (Au) working, platinum (Pt) counter and silver/silver chloride (Ag/AgCl) reference electrode) and a pre-molded polydimethylsiloxane (PDMS) plate (Supplementary Fig. 1). For the CRISPR/Cas13a system and catalyzed hairpin DNA circuit (Cas-CHDC)-powered RNA detection, all components are thoroughly mixed in a standard reaction vessel and incubated at 37 °C, allowing a two-stage signal amplification (Fig. 1B). The key component, linking the Cas-mediated target detection to the CHDC mechanism, is a specific single-stranded nucleic acid molecule called the "trigger". It consists of two functional domains: a uridine domain (rU-rU) acting as the 'fuse' point to be cleaved by the activated Cas13a, and an intermediary domain (1*-2*-3*), which, upon release, initiates the CHDC. Without the activated Cas13a, the trigger exhibits a stable hairpin structure in which the intermediary domain is locked. In the presence of target RNA, the guide sequence of the crRNA hybridizes with its target, Cas13a gets activated and cleaves multiple triggers at the 'fuse' points releasing numerous intermediary strands (primary amplification). Subsequently, specific binding of domain 1* (red) of the intermediary strand to the exposed domain 1 (red) of COMET-hairpin-1 (C–H1) initiates strand displacement to generate an intermediate complex (C–I1) through domain hybridization (1-2-3 and 3*-2*-1*). The released toehold domain 3* in C–I1 further triggers branch migration on domain 3-4*-3*-2* of COMET-hairpin-2 (C–H2) to form the C–H1–C–H2 duplex (C–I2), followed by displacement of the intermediary strand. The

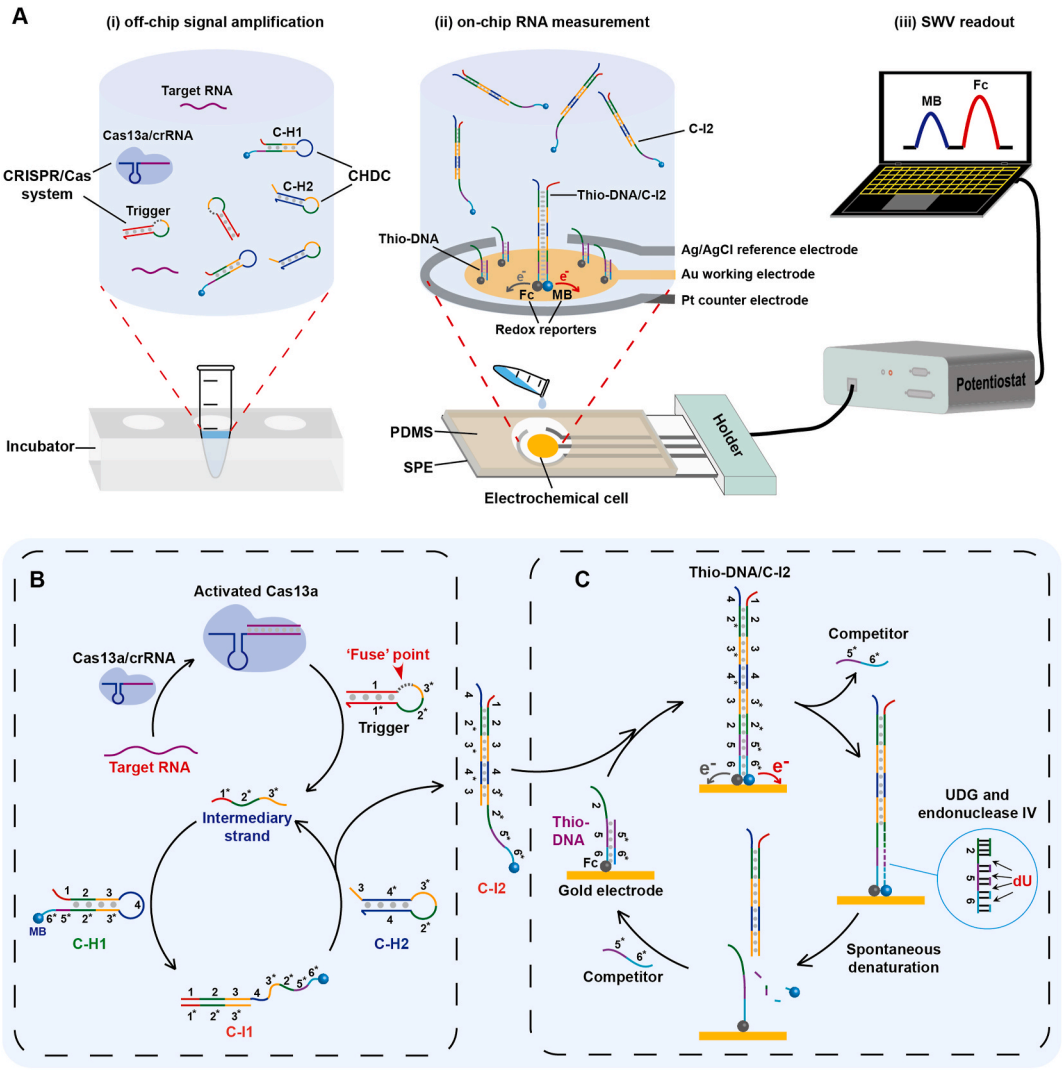

Fig. 1. Working principle of the Cas-CHDC-powered electrochemical RNA-sensing technology (COMET) chip. A) Stepwise operation of the COMET chip assay, which is composed of off-chip signal amplification (i), on-chip RNA measurements (ii), and square wave voltammetry (SWV) readout (iii). B) Schematic illustration of the Cas-CHDC system consisting of the Cas13a/crRNA complex, trigger as well as C–H1 and C–H2 for a two-stage signal amplification. Recognition of target RNA activates Cas13a, which then collaterally cleaves multiple triggers at their 'fuse' points to release the intermediaries, which in turn catalyze the hybridization of C–H1 and C–H2 through toehold-mediated strand displacement reactions for multiple cycles, generating numerous C–I2 molecules. C) Ratiometric correction using two redox reporters, and a cycle for enzymatic regeneration of the Thio-DNA monolayer on the gold electrode surface. C–I2 binds to the surface Thio-DNA, forming a Thio-DNA/C–I2 complex which allows electrochemical current enhancement between the electrode and the redox reporters (MB and Fc) (upper). After the measurement, the electrode is incubated in the enzyme mixture of UDG and endonuclease IV (right). Cleavage of the DNA backbone occurs at strategically placed deoxyuridines (dU). The resulting shorter DNA sections spontaneously denature and are washed away in buffer (lower), leaving only the surface Thio-DNA monolayer that is then ready for sample loading and another measurement.

latter will then start the next catalytic cycle to form another C–I2 strand (secondary amplification).

To counteract the aforementioned baseline drift between measurements, we used a ratiometric correction method which employs two independent redox reporters: methylene blue (MB) and ferrocene (Fc). MB is conjugated to the 3′ end of C–H1 and works as a sensing reporter, whereas Fc is conjugated to the 5' end of the Thio-DNA and works as a reference reporter. As shown in Fig. 1C, the Thio-DNA monolayer was pre-assembled on the gold electrode surface, the distance between the Fc and the gold electrode is thereby kept constant. Therefore, Fc is expected to serve as an internal control. Once C–I2 (2*-5*-6*) hybridizes to the surface Thio-DNA (2-5-6) and thereby displaces the competitor strand (5*-6*), MB gets closer to the gold electrode surface. Under the fixed concentration of other complexes that are involved in the reaction scheme, the number of Thio-DNA/C–I2 complexes is proportional to the amount of target RNA in the solution, which makes the electron transfer reactions between the electrode and the redox reporters (MB and Fc) indicative of the abundance of target RNA within the sample (Fig. 1C, upper). For the square wave voltammetry (SWV) readout, the COMET chip is placed into a custom-made chip-holder, connecting it to a potentiostat.

To successfully perform multiple RNA measurements consecutively using a single biosensor, enzymatic regeneration of the gold electrode surface was employed in this work. As depicted in the magnified circle in Fig. 1C (right) and Supplementary Fig. 2, the deoxyuridine ('dU') moieties in the 2*-5*-6* domain of the Thio-DNA/C–I2 complex are subject to enzymatic cleavage by the mixture of Uracil-DNA glycosylase (UDG) and endonuclease IV. In this way, the 2*-5*-6* domain of the Thio-DNA/C–I2 complex is enzymatically broken into four shorter segments of DNA. As a consequence, the Thio-DNA/C–I2 complex denatures to release the C–I2 fragments (Fig. 1C, lower), leaving only the Thio-DNA monolayer at the electrode surface (Fig. 1C, left). The images acquired

by atomic force microscopy (AFM) display the gold electrode surface during the enzymatic regeneration process (Supplementary Fig. 3). Through this gentle enzymatic mechanism, the gold electrode is regenerated in a matter of minutes and ready for the next measurement.

2.2. Feasibility of the Cas-CHDC amplification system

We first combine the collateral cleavage activity of Cas13a with the enzyme-free allosteric catalysis of CHDC to generate a two-stage amplification for a robust gain in current signals. Since triggers are the link connecting the two amplification stages, design and optimization of the trigger chain are essential for successful signal amplification. As the stem-to-loop ratio is the key factor determining the stability and functionality of the triggers, a series of six triggers with varied stem-to-loop ratios (Trigger-1 (8:16), Trigger-2 (9:15), Trigger-3 (12:12), Trigger-4 (14:10), Trigger-5 (16:8) and Trigger-6 (18:6)) were designed and synthesized (Supplementary Table 2). To test the capability of these 6 triggers to initiate CHDC, we employed Ribonuclease A (RNase A) mediated cleavage and determined the product (C–I2) by evaluating its band density using 10% polyacrylamide gel electrophoresis (PAGE) analysis. In order to obtain the optimal C–H1:C–H2 ratio, kinetics of CHDC were first monitored with C–H1 and fluorescence labeled C–H2 ($C–H2_{QF}$). The results revealed an elevated fluorescence intensity when increasing C–H1:$C–H2_{QF}$ from 0.25:1 to 1:1, whereas a slight decrease from 1:1 to 2:1 was observed ($C–H2_{QF}$ = 200 nM) (Fig. 2A). When C–H1 was kept at 200 nM, the background signal increased proportionally to the increased $C–H2_{QF}$ (Supplementary Fig. 4). Thus, the optimized C–H1:C–H2 ratio (1:1) was chosen based on the high reaction rate and low background.

PAGE analysis revealed that Trigger-1 to 3 can catalyze almost all C–H1 and C–H2 strands to produce numerous C–I2 molecules (L1, L3 of Supplementary Fig. 5 and L1 of Fig. 2B). By contrast, the catalytic effect gradually weakened from Trigger-4 to 6 (L3, L5 and L7 of Fig. 2B). However, in the absence of RNase A, Trigger-1 and Trigger-2 can also initiate CHDC and generate some C–I2, producing the risk of obtaining 'false positive' results (L2 and L4 of Supplementary Fig. 5). Finally, the collateral cleavage activity of CRISPR/Cas13a was assessed through real-time monitoring of the fluorescence emitted from cleaved QF-RNAs

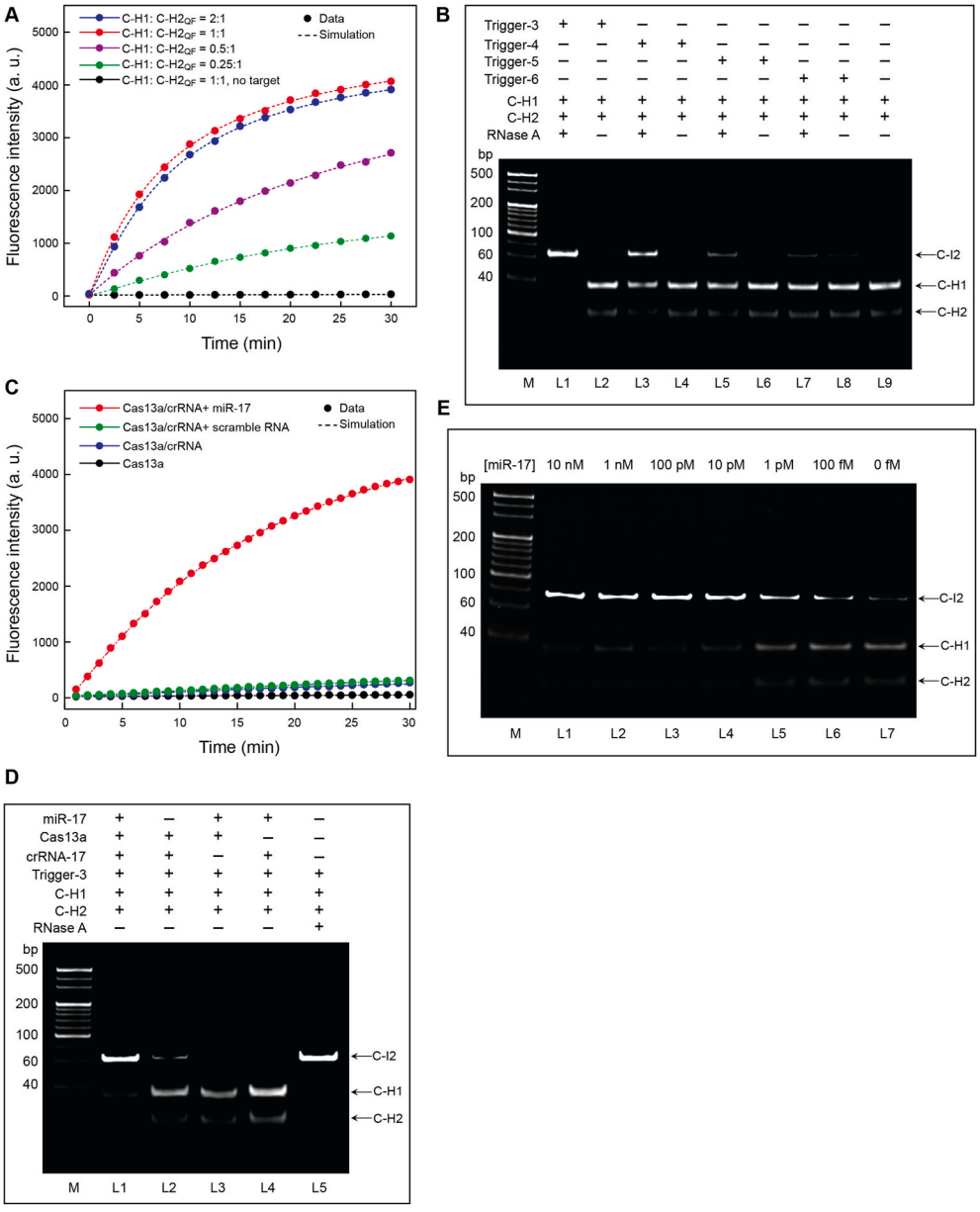

Fig. 2. Proof-of-principle of the Cas-CHDC system. A) The effect of different C–H1: C–H2 ratios on the catalyzed hairpin DNA circuit (CHDC) (C–H2 = 200 nM). B) Electrophoretic analysis of the capability of triggers to initiate the CHDC: Trigger-3 showed by far the strongest C–I2 band, whereas the catalytic effect gradually weakened from Trigger-4 to 6. C) Real-time fluorescence curves of the Cas13a mediated cleavage assay. Only in the presence of target miR-17, Cas13a shows perfect activity under the guidance of crRNA-17. D) Electrophoretic analysis of the capability of Cas-CHDC for miR-17 detection. Besides the positive control group (L5), only the Cas-CHDC group (L1) showed an obvious C–I2 band. E) Electrophoretic analysis of the target concentration dependent two-stage amplification of Cas-CHDC. A proportional relation between the density of the C–I2 and the concentration of miR-17 (100 fM to 10 nM) was observed. (M: Oligonucleotide ladder, '+' means presence, '-' means absence.).

(Fig. 2C). The experiment group with target (miR-17) showed a rapid increase in fluorescence intensity reaching 12.6 times the control value obtained from scramble RNA after 30 min.

Trigger-3 was selected for validation of the Cas-CHDC system since it showed the best performance initiating the CHDC. Both the Cas-CHDC group (Fig. 2D; L1) and the positive control group (Fig. 2D; L5) showed a strong C–I2 band, while the control group, not containing the target (miR-17), only had a weak C–I2 band (Fig. 2D; L2). Control groups containing neither crRNA (Fig. 2D; L3) nor Cas13a (Fig. 2D; L4) did not show C–I2 bands. In Fig. 2E, various concentrations of target miR-17 (100 fM to 10 nM) were measured using the Cas-CHDC system. The gel image reveals a directly proportional relation between the density of the C–I2 band and the concentration of miR-17, with an obvious C–I2 band at a miR-17 concentration as low as 100 fM (Fig. 2E; L6).

2.3. Successive and sensitive RNA detection on the COMET chip

We next integrate amplification by Cas-CHDC into a reusable electrochemical biosensing technology on a chip to realize rapid and highly sensitive RNA detection on a miniaturized POC testing device. To assess the reusability of the COMET chip, 45 repeated miR-17 (50 pM) measurements were carried out on a single chip. Fig. 3A shows the typical oxidation peaks of MB (−0.21 V vs. Ag/AgCl) and Fc (0.43 V) read out by SWV in the 1st, 20th and 45th test. For MB alone, similar to the electrochemical biosensor with only a single reporter, the oxidation peaks gradually decreased with increasing numbers of measurements resulting in a variability of 34.8%. However, application of the ratiometric correction (I_{MB}/I_{Fc}) exhibited an average response of 0.61 and drastically reduced this variability to 2.2% (Fig. 3B). We observed that at least 37 successive and stable measurements could be achieved on one single COMET chip (Fig. 3B; area highlighted in red).

Fig. 3C shows the SWV curves of MB and Fc in the presence of varying amounts of miR-17 (0.5 fM – 5 nM) and PBS as background signal, all measured at the 6-min time point. The MB oxidation peaks display a gradual increase in current signal proportional to the concentrations of target (miR-17), whereas the signal response of Fc does not show an obvious change at varied concentrations of miR-17. Using direct electrochemical readout at room temperature, the COMET chip was capable of detecting miR-17 levels as low as 0.5 fM, with a dynamic range extending to 5 nM. A calibration curve revealed that the I_{MB}/I_{Fc} increased proportionally to the miR-17 concentration (0.5 fM - 5 nM) (Fig. 3D). By fitting the measured data points to a four-parametric sigmoidal curve, the limit of detection (LOD) for miR-17 was identified at 50 aM, showing its capability to detect attomolar concentrations of RNAs, while consuming sample/reagent volumes of less than 10 μL per reaction in a readout time of no more than 6 min.

2.4. Target specificity of the COMET chip

To assess the specificity of the COMET chip, we challenged it by distinguishing the target RNA from other RNAs with one to several base

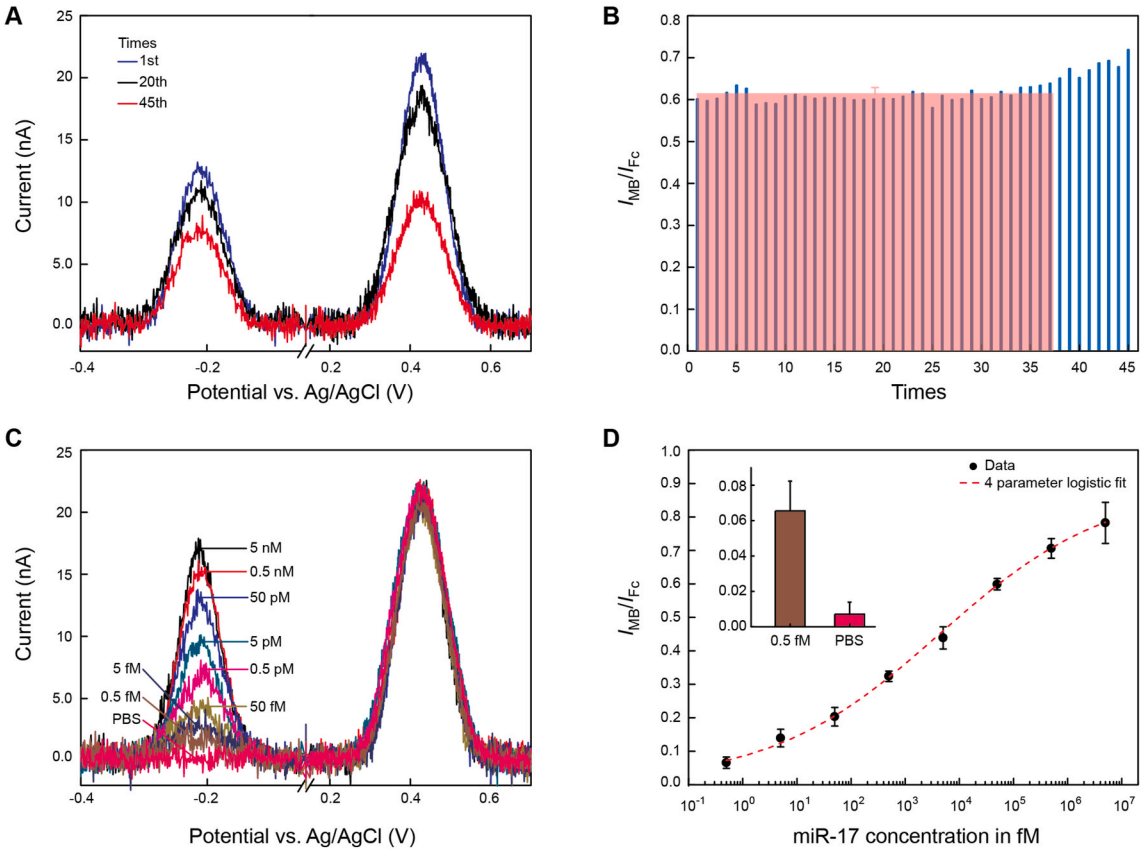

Fig. 3. Repeated and sensitive RNA detection on the COMET chip. A) Characteristic oxidation peaks of MB and Fc using SWV at three different measurement cycles: 1st (blue line), 20th (black line) and 45th (red line). B) Reliability between repeated measurements on the COMET chip. I_{MB}/I_{Fc} refers to the current ratio of MB and Fc. The blue histogram represents the signal responses of a set of measurements comprising 45 consecutive cycles. The red area highlights 37 successive stable measurements performed on one single chip. C) SWV scans for miR-17 quantification in the sub-fM to nM range. miR-17 with 500 nM was first quantified by Nanodrop, and then a serial dilution (0.5 fM – 5 nM) was performed. The COMET chip's response was proportional to miR-17 throughout all measurements, indicating high precision of the developed method. D) miR-17 calibration curves for the COMET chip. Concentrations as low as 0.5 fM were detected, with a dynamic range up to 5 nM. The results are fitted with a four-parametric logistic fit, resulting in a limit of detection of 50 aM. Error bars represent standard deviations. (For interpretation of the references to color in this figure legend, the reader is referred to the Web version of this article.)

mismatches. Compared to the MB oxidation peak recorded for 5 pM of miR-17, there was nearly no response for miR-155 or TTF-1 mRNA, which were applied in the same concentration. The I_{MB}/I_{Fc} of miR-17 was 7.8 and 6.8-fold higher than that of miR-155 and TTF-1 mRNA, respectively (Fig. 4A). Similar results were obtained in the case of miR-155 (Fig. 4B) and TTF-mRNA (Fig. 4C) when used as targets, respectively. miR-17 belongs to the miR-17/92 cluster family and since members of the same miRNA family often differ in only 1–2 bases, their respective unambiguous identification can be rather challenging. However, when targeting miR-17, the COMET chip was able to distinguish the RNA of interest from non-target RNAs of the same family: miR-106a (1-base mismatch), miR-20a and miR-20b (2-base mismatches) ($p < 0.0001$) (Fig. 4D). As shown in Supplementary Fig. 6, one additional synthetic mismatch within the guide region of the crRNA can cause an 'open-tail' or 'bulges' in the crRNA/target complex, which will severely reduce activation of Cas13a, and hence allow for robust RNA discrimination down to a single-base mismatch.

Next, we test the COMET chip's ability to detect low abundance target RNAs in complex samples, which is critical for future clinical application due to the high expression of non-target RNAs in patient blood. The test was performed in mixtures of target (miR-17) and non-target RNAs (miR-155, TTF-1 mRNA or their mixture) at a 1:1000 M ratio (50 fM of miR-17 and 50 pM non-target RNAs) (Fig. 4E). We found that the COMET chip could detect miR-17 at zeptomole amounts and as low as 0.1% of background RNA mixture. Besides, there is no significant difference in electrochemical readout of solutions containing either only miR-17 or miR-17 within a matrix of different RNAs.

2.5. RNA analysis in serum samples of lung cancer patients

To investigate the potential clinical utility of the COMET chip in NSCLC diagnosis, we herein employ it to evaluate the abundance of miR-17, miR-155 and TTF-1 mRNA in serum samples from 30 healthy subjects (male/female = 1.5), 12 patients with benign lung disease (BLD, male/female = 1.4), 20 early-stage (stage I-II, male/female = 1) and 55 late-stage (stage III-IV, male/female = 1.75) NSCLC patients with similar age (Supplementary Table 4). The total RNA from the serum samples was isolated and purified, using a commonly available RNA purification kit. First, to assess the risk of crosstalk between measurements of serum samples from NSCLC patients, miR-17, miR-155 and

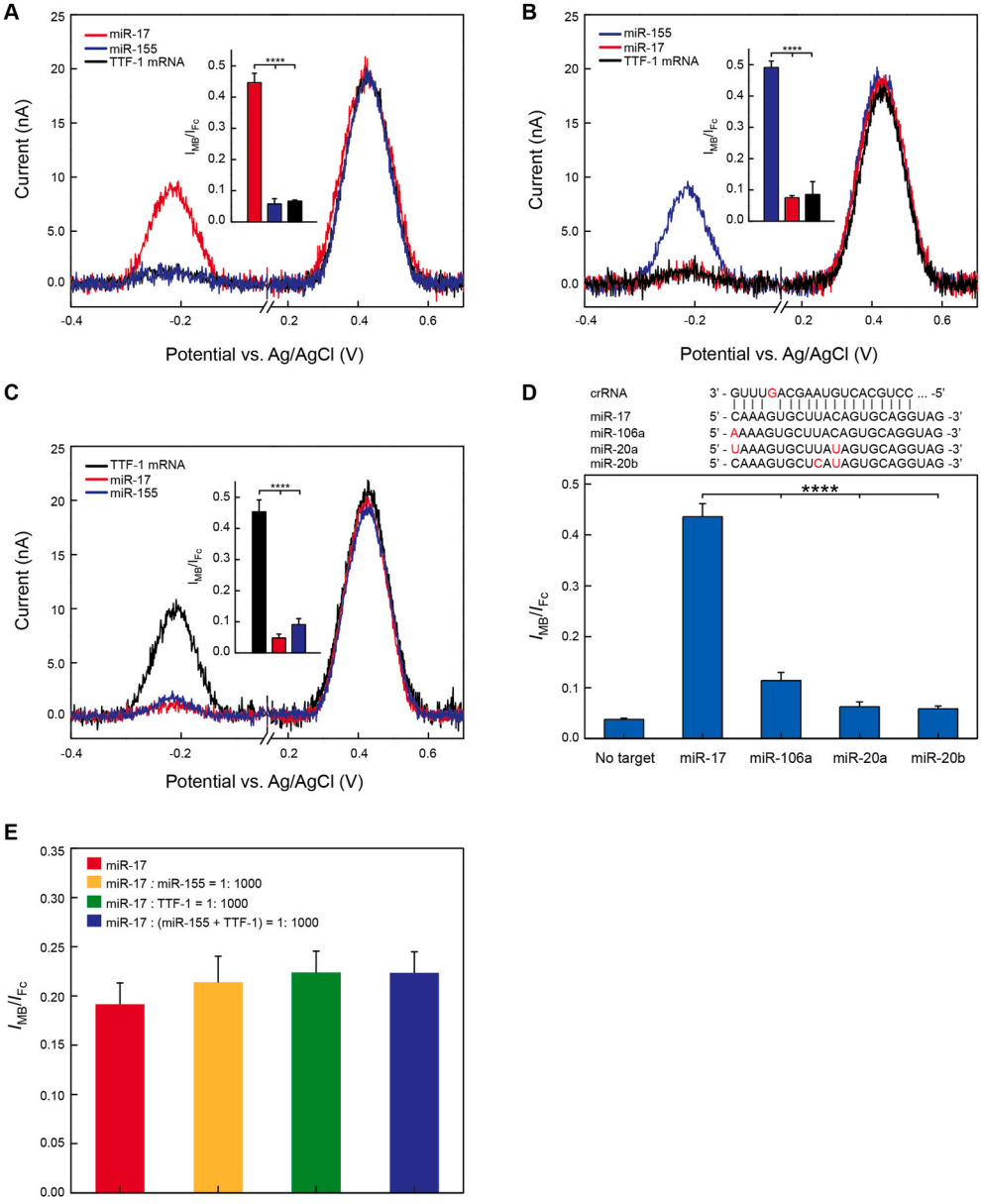

Fig. 4. Target specificity of the COMET chip. A) Only the target (miR-17) generated measurable responses, while there was no response for miR-155 or TTF-1 mRNA (several mismatches). Similar results were obtained in the case of miR-155 (B) and TTF-1 mRNA (C), when used as targets, respectively. crRNA-17, crRNA-155, crRNA-TTF1 were designed to target miR-17, miR-155 and TTF-1 mRNA (5 pM each) respectively. D) crRNA guide region of crRNA-17 with a synthetic mismatch complementary to miR-17 used for improved specificity. The mismatches in crRNA or target sequences are highlighted in red (upper). Linear scale comparison of target miR-17, miR-106a (single mismatch), miR-20a and miR-20b (two mismatches) detected by the COMET chip, respectively (lower). E) miR-17 constitutes 0.1% of the RNA mixture (the initial miR-17 concentration of 50 fM was kept constant throughout these measurements). (Paired two tailed Student's t test, $^{****}P < 0.0001$). (For interpretation of the references to color in this figure legend, the reader is referred to the Web version of this article.)

TTF-1 mRNA (in the same sample (Fig. 5A)), and miR-17 (in four different samples (Fig. 5B)) were determined by turns on a single chip in triplicate, respectively. Also, the measurements of miR-17, miR-155 and TTF-1 mRNA (in the same sample) were carried out by turns on 5 individual chips (Supplementary Fig. 7). The results show little variability between measurements and no crosstalk between serum samples. COMET analysis revealed that I_{MB}/I_{Fc} of miR-17, miR-155 and TTF-1 in serum samples effectively allows discrimination of late-stage NSCLC patients from healthy subjects ($p < 0.0001$), while there was no obvious distinction between BLD patients and early-stage NSCLC patients (Fig. 5C, D and E). Besides, an overlap of I_{MB}/I_{Fc} was observed between early-stage NSCLC patients and healthy subjects (miR-17: $p < 0.05$, miR-155: $p < 0.01$, TTF-1 mRNA: $p < 0.001$), early- and late-stage NSCLC patients (miR-17: $p < 0.1$, miR-155: $p < 0.001$, TTF-1 mRNA: $p < 0.01$), BLD patients and late-stage NSCLC patients (miR-17: $p < 0.05$, miR-155: $p < 0.0001$, TTF-1 mRNA: $p < 0.001$). Based on these results, none of the three RNAs can be handled as an effective biomarker of NSCLC by itself.

However, when treated as an entity (3-RNA set I), the performance of the RNAs (miR-17, miR-155 and TTF-1 mRNA) drastically improves. Visualization in a 3-dimensional dot chart revealed that 3-RNA set I could effectively distinguish early- and late-stage NSCLC patients from healthy subjects ($p < 0.0001$, Fig. 5F). The BLD patients exhibit a slightly higher 3-RNA set I expression than healthy subjects ($p < 0.05$), followed by early-stage NSCLC patients ($p < 0.01$, compared to BLD patients) and finally late-stage NSCLC patients, whose 3-RNA set I is strongly elevated ($p < 0.0001$), compared to early-stage NSCLC patients. Receiver operating characteristic (ROC) curves for the 3-RNA set I shows area under curve (AUC) values of 0.923 (sensitivity = 90.7%, specificity = 88.1%) and 0.810 (sensitivity = 80%, specificity = 85.7%) in NSCLC patients (stage I-IV) and early-stage NSCLC patients (stage I-II) compared to non-cancer cohorts (healthy subjects and BLD patients), respectively. (Fig. 5I and J and Supplementary Tables 5 and 6).

3 more RNAs (miR-19b, miR-210 and EGFR mRNA) were employed to improve discrimination of the serum samples ($n = 10$), including 1 healthy donor, 3 BLD patients, 4 early- and 2 late-stage NSCLC patients, for which classification into the cohorts was not accomplishable on the basis of the above 3-RNA set I (Fig. 5G). Except for 1 BLD patient and 2 early-stage NSCLC patients, all 7 samples could be effectively classified (Fig. 5H). Overall, inclusion of the additional 3-RNA set II (miR-19b, miR-210 and EGFR mRNA) into the existing 3-RNA set I (miR-17, miR-155 and TTF-1 mRNA) improves the AUC value to 0.977 (sensitivity = 97.3%, specificity = 95.2%) for distinguishing NSCLC patients (stage I-IV) from non-cancer cohorts (Fig. 5I and Supplementary Table 5). Notably, the 6-RNA set (3-RNA set I and 3-RNA set II) shows an AUC value of 0.927 in early-stage NSCLC patients compared to non-cancer cohorts, with a sensitivity of 90% and specificity of 95.2% (Fig. 5J and Supplementary Table 6). Finally, the validation experiment for COMET (a performance comparison with qRT-PCR) was performed by targeting the 3-RNA set I (miR-17, miR-155 and TTF-1 mRNA) in 10 randomly selected serum samples (Fig. 5K and Supplementary Fig. 8). Compared with COMET, qRT-PCR is inferior in classifying NSCLC patients of stage I-IV from non-cancer cohorts. COMET provides a more significant distinction ($p < 0.001$) between early-stage NSCLC patients and non-cancer cohorts than qRT-PCR ($p < 0.05$). Taken together, the COMET chip proves to be a promising tool for early-stage cancer detection.

3. Discussion

mRNAs and miRNAs in the bloodstream are promising biomarkers for minimally invasive cancer diagnostics. However, most methods for nucleic acid analysis require sophisticated measurement devices/systems and extensive sample preparation, a lengthy hands-on time and well-trained operators. In addition, the detection of nucleic acids mostly relies on the use of bulky and expensive equipment, which is difficult to access at the POC. Here, we present a facile fusion of CRISPR/Cas and CHDC with a reusable electrochemical biosensor for the rapid detection of multiple RNAs with high sensitivity and selectivity in serum specimens, while also enabling a miniaturization for clinical practice.

For the off-chip two-stage signal amplification, the Cas13a-mediated collateral cleavage of trigger molecules and the enzyme-free allosteric catalysis of CHDC were performed in one pot. We have recently demonstrated the CRISPR-powered electrochemical biosensing to be a low-cost, easily scalable, and target amplification-free tool for miRNA diagnostics (Bruch et al., 2019a). In this work, CHDC, an enzyme-free signal amplifier relying on hybridization and strand-exchange reactions, has been employed to further increase the sensitivity for detecting low expression RNAs in serum of NSCLC patients. By our unique combination of the CRISPR/Cas13a system with the CHDC, the LOD of our system could be drastically reduced to attomolar concentrations. COMET enables the RNA detection with a broad dynamic range of 8 orders of magnitude (50 aM to 5 nM), which surpasses the performance of the representative CRISPR/Cas13a methods, e.g., SHERLOCK (2–3 orders of magnitude) (East-Seletsky et al., 2016; Gootenberg et al., 2017). The impressive dynamic range of COMET allows directly quantitative measurement of target RNA in clinical samples, providing enhanced flexibility in sample preparation (Weber et al., 2010). Among all components, triggers are well-designed, containing two functional domains (rU-rU and 1*-2*-3*) to link the two stages of amplification. The trigger's rU-rU is a single-stranded RNA and located in the loop region for two reasons: first, the activated Cas13a only cleaves single-stranded RNAs and prefers to cut uridines, but does not work on double-stranded RNAs or DNA/RNA dimers (Liu et al., 2017). Second, rU-rU, as unmatched ssRNA bulge structure, if introduced into the stem region, will increase the Gibbs free energy (ΔG) and decrease its melting temperature (T_m), consequently disrupt cohesion of the stem's structure and affect stability of the whole trigger chain (Supplementary Fig. 9). Once rU-rU is cut, the trigger's 1*-2*-3* is released as a single-stranded nucleic acid which will initiate the allosteric catalysis of CHDC.

A dual-reporter (MB and Fc) approach was employed to perform baseline drift correction for the on-chip electrochemical measurements. MB and Fc were chosen because they are energetically stable, similar in their physical properties, and exhibit no overlap in their oxidation potentials (Du et al., 2014). This ratiometric correction approach largely reduced drift in the raw current signals from up to 34.8% to less than 2.2%. Given this result, we are optimistic that robust and reproducible signals are provided by the dual-reporter drift correction. Besides, enzymatic regeneration of the surface Thio-DNA was employed between measurements to realize reusability of biosensors. The COMET chip's electrode surface can be regenerated very easily (one-step) and rapidly (7 min), while up to 37 measurements in sequence can be achieved without loss of assay sensitivity. Its overall processing time for one measurement is only 36 min including a 6-min readout time. Notably, the developed reusable biosensor can fully regenerate the sensing interface, eliminating the risk of crosstalk between measurements or patient samples. These characteristics could make COMET a pioneer for a new generation of RNA diagnostic tools. When challenged with serum samples of various test populations (total $n = 117$), the COMET chip revealed the necessity of a set of multiple RNAs in order to achieve an accurate diagnosis of diseases, especially for early-stage cancer. The accuracy, sensitivity and specificity of COMET based on a panel of six RNAs to detect NSCLC patients at stage I-II are 92.7%, 90% and 95.2%, respectively. We plan to conduct a large-scale multi-site validation study to establish a relatively accurate threshold for on-site clinical use. The COMET technology harbors the potential to further be engineered and reconfigured in combination with other strategies, such as microfluidic platforms, to realize signal amplification and simultaneous detection of multiple RNAs on one chip, producing a high-efficiency 'one-for-all' biosensor.

Although COMET is performed in two steps (off-chip and on-chip), and the guide sequence of the crRNA needs to be redesigned and synthesized according to various target sequences, it does not require

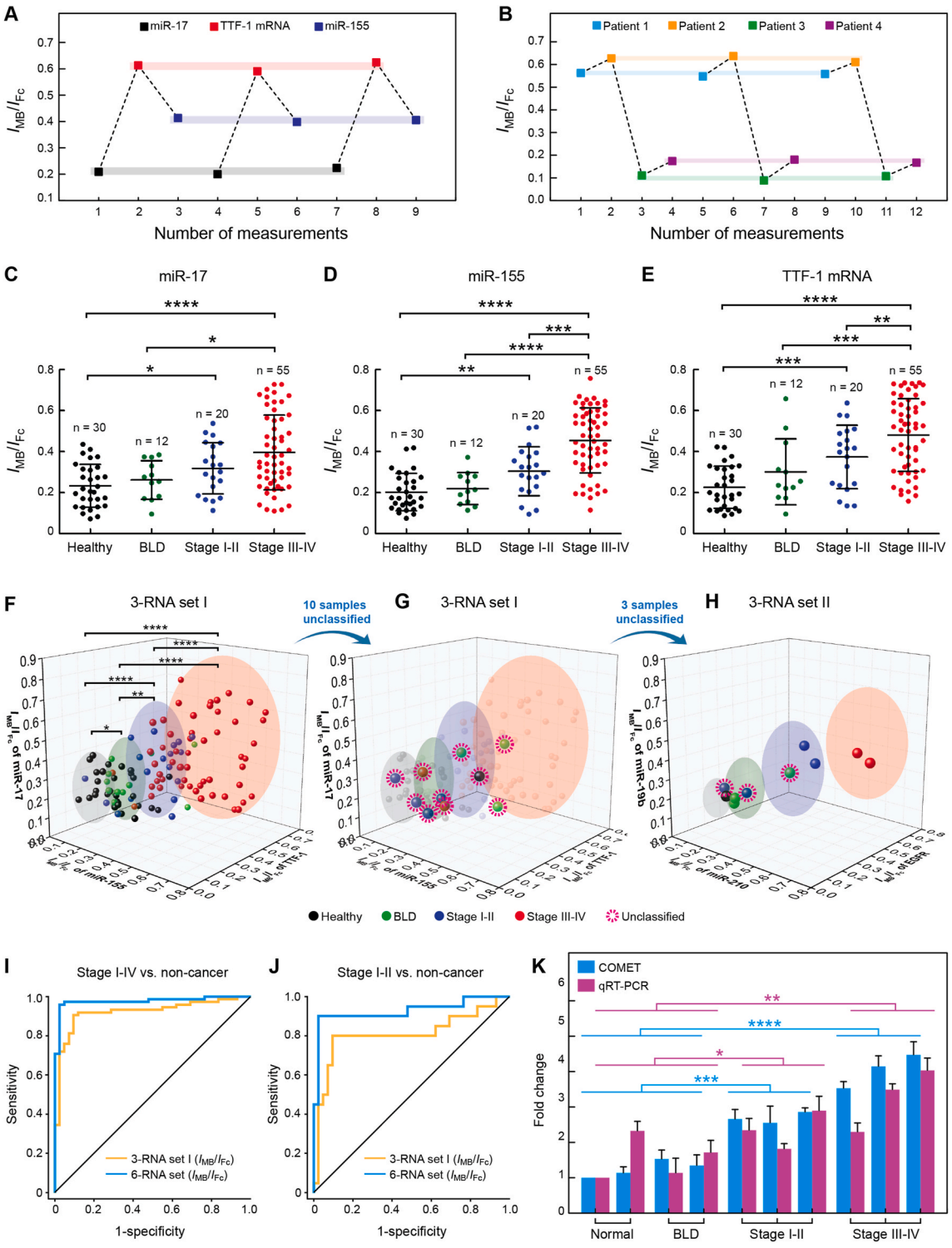

Fig. 5. Successive measurements of multiple-RNAs in serum samples. A) The I_{MB}/I_{Fc} for miR-17, miR-155 and TTF-1 mRNA in the same serum sample of an NSCLC patient, determined by turns in triplicate using COMET. B) The I_{MB}/I_{Fc} for miR-17 in four randomly selected serum samples of NSCLC patients, determined by turns in triplicate using COMET. C) The I_{MB}/I_{Fc} for miR-17 in the serum of healthy subjects (n = 30), BLD patients (n = 12), NSCLC patients at stage I-II (n = 20), and stage III–IV (n = 55), determined using COMET. D) The I_{MB}/I_{Fc} for miR-155 of the four cohorts (n = 117), determined using COMET. E) The I_{MB}/I_{Fc} for TTF-1 mRNA of the four cohorts, determined using COMET. F) 3-Dimensional dot chart of I_{MB}/I_{Fc} for 3-RNA set I (miR-17, miR-155 and TTF-1 mRNA) for all four cohorts. G) 10 serum samples out of four cohorts unclassified by 3-RNA set I, including healthy subjects (n =1), BLD patients (n = 3), NSCLC patients at stage I-II (n = 4), and stage III–IV (n = 2). H) 3-Dimensional dot chart of I_{MB}/I_{Fc} for 3-RNA set II (miR-19b, miR-210, EGFR mRNA) for these 10 serum samples. I) Receiver operating characteristic (ROC) curve analysis of the 3-RNA set I and 6-RNA set (miR-17, miR-155, TTF-1 mRNA, miR-19b, miR-210 and EGFR mRNA) for discriminating NSCLC patients at stage I-IV (n = 75) from non-cancer cohorts (healthy subjects and BLD patients, n = 42), respectively. J) ROC curve analysis of 3-RNA set I and 6-RNA set for discriminating NSCLC patients at stage I-II (n = 20) from non-cancer cohorts (n = 42), respectively. K) Comparison of COMET with qRT-PCR by targeting 3-RNA set I in 10 randomly selected serum samples from four cohorts, including 2 healthy subjects, 2 BLD patients, 3 early-stage and 3 late-stage NSCLC patients. (Paired two tailed Student's t test, $^{*}P < 0.05$, $^{**}P < 0.01$, $^{***}P < 0.001$, $^{****}P < 0.0001$).

complex nucleic acid amplification procedures, sophisticated equipment or especially trained personnel, which are needed for most of the current nucleic acid detection techniques. It is worth noting that the total cost of the chip and employed reagents can be as low as $0.27 per test (Supplementary Table 7). This new technology provides advantages including high sensitivity, low-cost, easy scalability and short assay time. Overall, the COMET system could be implemented in a routine POC diagnostic setting of early-stage cancer as well as in therapeutic monitoring.

Author contributions

J.H., C.D. and T.K. directed the research. J.H. and Y. Sheng conceived the idea. Y. Sheng, T.Z., S.Z., X.Z., Y. Shan, T.L. and Z.H. performed the experiments. J.H., Y. Sheng, T.Z., M.J. and C.D. analyzed the data and wrote the paper. F.Q., Z.X., Y.A. and H.Z. assisted with data interpretation. C.D., M.J. and G.U. commented and revised the paper.

CRediT authorship contribution statement

Yan Sheng: Methodology, Conceptualization, Validation, Formal analysis, Investigation, Resources, Writing - original draft. **Tenghua Zhang:** Investigation, Formal analysis, Writing - original draft. **Shihong Zhang:** Validation, Investigation, Formal analysis. **Midori Johnston:** Investigation, Formal analysis, Writing - review & editing. **Xiaohe Zheng:** Investigation. **Yuanyue Shan:** Investigation. **Tong Liu:** Investigation. **Zena Huang:** Investigation. **Feiyang Qian:** Formal analysis. **Zihui Xie:** Formal analysis. **Yiru Ai:** Formal analysis. **Hankang Zhong:** Formal analysis. **Tairong Kuang:** Writing - original draft, Supervision. **Can Dincer:** Formal analysis, Writing - review & editing, Supervision, Funding acquisition. **Gerald Anton Urban:** Writing - review & editing. **Jiaming Hu:** Methodology, Conceptualization, Formal analysis, Resources, Writing - review & editing, Supervision, Project administration, Funding acquisition.

Declaration of competing interest

The authors declare that they have no known competing financial interests or personal relationships that could have appeared to influence the work reported in this paper.

Acknowledgements

This work was supported financially by the National Natural Science Foundation of China (No. 21804023), Science and Technology Program of Guangzhou, China (No. 2019050001), Scientific Research Projects of Guangdong Province, China (No. 2019QN01Y725), Recruitment Program of Global Experts, China, Natural Science Foundation of Guangdong Province, China (No. 2018A030313319), the Scientific Research Projects of Guangzhou, China (No. 201805010002), and Fundamental Research Funds for the Provincial Universities of Zhejiang (No. RF-A2020008). C.D. and M.J. would like to thank the Deutsche Forschungsgemeinschaft (DFG, German Research Foundation) for the partially funding of this work under Grant No. 421356369.

Appendix A. Supplementary data

Supplementary data to this article can be found online at https://doi.org/10.1016/j.bios.2021.113027.

References

Bartel, D.P., 2004. MicroRNAs: genomics, biogenesis, mechanism, and function. Cell 116 (2), 281–297.
Bruch, R., Baaske, J., Chatelle, C., Meirich, M., Madlener, S., Weber, W., Dincer, C., Urban, G.A., 2019a. CRISPR/Cas13a-Powered electrochemical microfluidic biosensor for nucleic acid amplification-free miRNA diagnostics. Adv. Mater. 31 (51), 1905311.
Bruch, R., Johnston, M., Kling, A., Mattmüller, T., Baaske, J., Partel, S., Madlener, S., Weber, W., Urban, G.A., Dincer, C., 2021. Crispr-powered electrochemical microfluidic multiplexed biosensor for target amplification-free mirna diagnostics. Biosens. Bioelectron. 112887.
Bruch, R., Urban, G.A., Dincer, C., 2019b. CRISPR/Cas powered multiplexed biosensing. Trends Biotechnol. 37 (8), 791–792.
Bruch, R., Urban, G.A., Dincer, C., 2019c. Unamplified gene sensing via Cas9 on graphene. Nat. Biomed. Eng. 3 (6), 419–420.
Cai, D., Ren, L., Zhao, H., Xu, C., Zhang, L., Yu, Y., Wang, H., Lan, Y., Roberts, M.F., Chuang, J.H., Naughton, M.J., Ren, Z., Chiles, T.C., 2010. A molecular-imprint nanosensor for ultrasensitive detection of proteins. Nat. Nanotechnol. 5 (8), 597–601.
Chen, J.S., Ma, E., Harrington, L.B., Da Costa, M., Tian, X., Palefsky, J.M., Doudna, J.A., 2018. CRISPR-Cas12a target binding unleashes indiscriminate single-stranded DNase activity. Science 360 (6387), 436–439.
Chen, Q., Si, Q., Xiao, S., Xie, Q., Lin, J., Wang, C., Chen, L., Chen, Q., Wang, L., 2012. Prognostic significance of serum miR-17-5p in lung cancer. Med. Oncol. 30 (1), 353.
Dincer, C., Bruch, R., Kling, A., Dittrich, P.S., Urban, G.A., 2017. Multiplexed point-of-care testing-xPOCT. Trends Biotechnol. 35 (8), 728–742.
Dittrich, P.S., Manz, A., 2006. Lab-on-a-chip: microfluidics in drug discovery. Nat. Rev. Drug Discov. 5 (3), 210–218.
Doudna, J.A., Charpentier, E., 2014. The new frontier of genome engineering with CRISPR-Cas9. Science 346 (6213), 1258096.
Du, Y., Lim, B.J., Li, B., Jiang, Y.S., Sessler, J.L., Ellington, A.D., 2014. Reagentless, ratiometric electrochemical DNA sensors with improved robustness and reproducibility. Anal. Chem. 86 (15), 8010–8016.
East-Seletsky, A., O'Connell, M.R., Knight, S.C., Burstein, D., Cate, J.H.D., Tjian, R., Doudna, J.A., 2016. Two distinct RNase activities of CRISPR-C2c2 enable guide-RNA processing and RNA detection. Nature 538 (7624), 270–273.
Ferguson, B.S., Hoggarth, D.A., Maliniak, D., Ploense, K., White, R.J., Woodward, N., Hsieh, K., Bonham, A.J., Eisenstein, M., Kippin, T.E., Plaxco, K.W., Soh, H.T., 2013. Real-time, aptamer-based tracking of circulating therapeutic agents in living animals. Sci. Transl. Med. 5 (213), 213ra165-213ra165.
Gao, Y., Qiang, L., Chu, Y., Han, Y., Zhang, Y., Han, L., 2020. Microfluidic chip for multiple detection of miRNA biomarkers in breast cancer based on three-segment hybridization. AIP Adv. 10 (4).
Gootenberg, J.S., Abudayyeh, O.O., Kellner, M.J., Joung, J., Collins, J.J., Zhang, F., 2018. Multiplexed and portable nucleic acid detection platform with Cas13, Cas12a, and Csm6. Science 360 (6387), 439–444.
Gootenberg, J.S., Abudayyeh, O.O., Lee, J.W., Essletzbichler, P., Dy, A.J., Joung, J., Verdine, V., Donghia, N., Daringer, N.M., Freije, C.A., Myhrvold, C., Bhattacharyya, R.P., Livny, J., Regev, A., Koonin, E.V., Hung, D.T., Sabeti, P.C., Collins, J.J., Zhang, F., 2017. Nucleic acid detection with CRISPR-Cas13a/C2c2. Science 356 (6336), 438–442.
Gubala, V., Harris, L.F., Ricco, A.J., Tan, M.X., Williams, D.E., 2012. Point of care diagnostics: status and future. Anal. Chem. 84 (2), 487–515.
Guo, H., Ingolia, N.T., Weissman, J.S., Bartel, D.P., 2010. Mammalian microRNAs predominantly act to decrease target mRNA levels. Nature 466 (7308), 835–840.
Harrington, L.B., Burstein, D., Chen, J.S., Paez-Espino, D., Ma, E., Witte, I.P., Cofsky, J.C., Kyrpides, N.C., Banfield, J.F., Doudna, J.A., 2018. Programmed DNA destruction by miniature CRISPR-Cas14 enzymes. Science 362 (6416), 839–842.
Hausser, J., Zavolan, M., 2014. Identification and consequences of miRNA-target interactions–beyond repression of gene expression. Nat. Rev. Genet. 15 (9), 599–612.
Heller, A., Feldman, B., 2008. Electrochemical glucose sensors and their applications in diabetes management. Chem. Rev. 108 (7), 2482–2505.
Hu, J., Kuang, T., 2018. DNA-coded fluorescence for color painting RNAs. Inside Chem. 4 (6), 1194–1196.
Hu, J., Kwak, K.J., Shi, J., Yu, B., Sheng, Y., Lee, L.J., 2018. Overhang molecular beacons encapsulated in tethered cationic lipoplex nanoparticles for detection of single-point mutation in extracellular vesicle-associated RNAs. Biomaterials 183, 20–29.
Hu, J., Sheng, Y., Kwak, K.J., Shi, J., Yu, B., Lee, L.J., 2017. A signal-amplifiable biochip quantifies extracellular vesicle-associated RNAs for early cancer detection. Nat. Commun. 8 (1), 1683.
Hu, J., Wang, T., Kim, J., Shannon, C., Easley, C.J., 2012. Quantitation of femtomolar protein levels via direct readout with the electrochemical proximity assay. J. Am. Chem. Soc. 134 (16), 7066–7072.
Hu, J., Yu, Y., Brooks, J.C., Godwin, L.A., Somasundaram, S., Torabinejad, F., Kim, J., Shannon, C., Easley, C.J., 2014. A reusable electrochemical proximity assay for highly selective, real-time protein quantitation in biological matrices. J. Am. Chem. Soc. 136 (23), 8467–8474.
Jeffrey, S.S., 2008. Cancer biomarker profiling with microRNAs. Nat. Biotechnol. 26 (4), 400–401.
Konermann, S., Brigham, M.D., Trevino, A.E., Joung, J., Abudayyeh, O.O., Barcena, C., Hsu, P.D., Habib, N., Gootenberg, J.S., Nishimasu, H., Nureki, O., Zhang, F., 2015. Genome-scale transcriptional activation by an engineered CRISPR-Cas9 complex. Nature 517 (7536), 583–588.
Lee, H., Lee, J., Lee, S.-G., Doyle, P.S., 2020. Hydrogel-based colorimetric assay for multiplexed MicroRNA detection in a microfluidic device. Anal. Chem. 92 (8), 5750–5755.
Lee, L.J., Yang, Z., Rahman, M., Ma, J., Kwak, K.J., McElroy, J., Shilo, K., Goparaju, C., Yu, L., Rom, W., Kim, T.K., Wu, X., He, Y., Wang, K., Pass, H.I., Nana-Sinkam, S.P., 2016. Extracellular mRNA detected by tethered lipoplex nanoparticle biochip for lung adenocarcinoma detection. Am. J. Respir. Crit. Care Med. 193 (12), 1431–1433.

Li, H., Arroyo-Currás, N., Kang, D., Ricci, F., Plaxco, K.W., 2016. Dual-reporter drift correction to enhance the performance of electrochemical aptamer-based sensors in whole blood. J. Am. Chem. Soc. 138 (49), 15809–15812.
Li, S.-Y., Cheng, Q.-X., Wang, J.-M., Li, X.-Y., Zhang, Z.-L., Gao, S., Cao, R.-B., Zhao, G.-P., Wang, J., 2018. CRISPR-Cas12a-assisted nucleic acid detection. Cell Discov. 4 (1), 20.
Liu, C., Zhao, J., Tian, F., Cai, L., Zhang, W., Feng, Q., Chang, J., Wan, F., Yang, Y., Dai, B., Cong, Y., Ding, B., Sun, J., Tan, W., 2019. Low-cost thermophoretic profiling of extracellular-vesicle surface proteins for the early detection and classification of cancers. Nat. Biomed. Eng. 3 (3), 183–193.
Liu, L., Li, X., Ma, J., Li, Z., You, L., Wang, J., Wang, M., Zhang, X., Wang, Y., 2017. The molecular architecture for RNA-guided RNA cleavage by Cas13a. Cell 170 (4), 714–726 e710.
Muers, M., 2011. Transcriptome to proteome and back to genome. Nat. Rev. Genet. 12 (8), 518-518.
Nelles, David A., Fang, Mark Y., O'Connell, Mitchell R., Xu, Jia L., Markmiller, Sebastian J., Doudna, Jennifer A., Yeo, Gene W., 2016. Programmable RNA tracking in live cells with CRISPR/Cas9. Cell 165 (2), 488–496.
Pheeney, C.G., Guerra, L.F., Barton, J.K., 2012. DNA sensing by electrocatalysis with hemoglobin. Proc. Natl. Acad. Sci. Unit. States Am. 109 (29), 11528–11533.
Proudfoot, N.J., Furger, A., Dye, M.J., 2002. Integrating mRNA processing with transcription. Cell 108 (4), 501–512.
Santarius, T., Shipley, J., Brewer, D., Stratton, M.R., Cooper, C.S., 2010. A census of amplified and overexpressed human cancer genes. Nat. Rev. Canc. 10 (1), 59–64.
Seelig, G., Soloveichik, D., Zhang, D.Y., Winfree, E., 2006. Enzyme-free nucleic acid logic circuits. Science 314 (5805), 1585–1588.
Shen, J., Zhou, X., Shan, Y., Yue, H., Huang, R., Hu, J., Xing, D., 2020. Sensitive detection of a bacterial pathogen using allosteric probe-initiated catalysis and CRISPR-Cas13a amplification reaction. Nat. Commun. 11 (1), 267.
Treerattrakoon, K., Jiemsakul, T., Tansarawiput, C., Pinpradup, P., Iempridee, T., Luksirikul, P., Khoothiam, K., Dharakul, T., Japrung, D., 2019. Rolling circle amplification and graphene-based sensor-on-a-chip for sensitive detection of serum circulating miRNAs. Anal. Biochem. 577, 89–97.
Tsai, S.Q., Wyvekens, N., Khayter, C., Foden, J.A., Thapar, V., Reyon, D., Goodwin, M.J., Aryee, M.J., Joung, J.K., 2014. Dimeric CRISPR RNA-guided FokI nucleases for highly specific genome editing. Nat. Biotechnol. 32 (6), 569–576.
Vanlandewijck, M., He, L., Mäe, M.A., Andrae, J., Ando, K., Del Gaudio, F., Nahar, K., Lebouvier, T., Laviña, B., Gouveia, L., Sun, Y., Raschperger, E., Räsänen, M., Zarb, Y., Mochizuki, N., Keller, A., Lendahl, U., Betsholtz, C., 2018. A molecular atlas of cell types and zonation in the brain vasculature. Nature 554 (7693), 475–480.
Weber, J.A., Baxter, D.H., Zhang, S., Huang, D.Y., Huang, K.H., Lee, M.J., Galas, D.J., Wang, K., 2010. The microRNA spectrum in 12 body fluids. Clin. Chem. 56 (11), 1733–1741.
Wickramasinghe, V.O., Laskey, R.A., 2015. Control of mammalian gene expression by selective mRNA export. Nat. Rev. Mol. Cell Biol. 16 (7), 431–442.
Xue, X., Liu, Y., Wang, Y., Meng, M., Wang, K., Zang, X., Zhao, S., Sun, X., Cui, L., Pan, L., Liu, S., 2016. MiR-21 and MiR-155 promote non-small cell lung cancer progression by downregulating SOCS1, SOCS6, and PTEN. Oncotarget 7 (51), 84508–84519.
Yanaihara, N., Caplen, N., Bowman, E., Seike, M., Kumamoto, K., Yi, M., Stephens, R.M., Okamoto, A., Yokota, J., Tanaka, T., Calin, G.A., Liu, C.-G., Croce, C.M., Harris, C.C., 2006. Unique microRNA molecular profiles in lung cancer diagnosis and prognosis. Canc. Cell 9 (3), 189–198.
Zaporozhchenko, I.A., Morozkin, E.S., Ponomaryova, A.A., Rykova, E.Y., Cherdyntseva, N.V., Zheravin, A.A., Pashkovskaya, O.A., Pokushalov, E.A., Vlassov, V.V., Laktionov, P.P., 2018. Profiling of 179 miRNA expression in blood plasma of lung cancer patients and cancer-free individuals. Sci. Rep. 8 (1), 6348.
Zhang, D.Y., Turberfield, A.J., Yurke, B., Winfree, E., 2007. Engineering entropy-driven reactions and networks catalyzed by DNA. Science 318 (5853), 1121–1125.
Zhu, X., Feng, C., Ye, Z., Chen, Y., Li, G., 2014. Fabrication of magneto-controlled moveable architecture to develop reusable electrochemical biosensors. Sci. Rep. 4 (1), 4169.